Interpolated Average CT for Attenuation Correction in PET – A Simulation Study

Greta S. P. Mok, *Member, IEEE*, Tao Sun, Tung-Hsin Wu, Mu-Bai Chang and Tzung-Chi Huang

Abstract–**Previously we proposed using an interpolated average CT (IACT) method for attenuation correction (AC) in PET, which is a good low-dose approximation of cine average CT (CACT) to reduce misalignments and improve quantification in PET/CT. This study aims to evaluate the performance of IACT for different motion amplitudes. We used the digital 4D Extended Cardiac Torso phantom (XCAT) to simulate maximum of 2 cm, 3 cm and 4 cm respiratory motions. The respiratory cycle was divided into 13 phases, with average activity and attenuation maps to represent ^{18}F-FDG distribution with average respiratory motions and CACT respectively. The end-inspiration, end-expiration and the mid-respiratory phases represented 3 different helical CTs (HCT-1, HCT-5 and HCT-8). The IACTs were generated using: (a) 2 extreme + 11 interpolated phases ($IACT_{2o11i}$); (b) 2 phases right after the extreme phases + 11 interpolated phases ($IACT_{2s11i}$); (c) 4 original + 9 interpolated phases ($IACT_{4o9i}$). A spherical lesion with target-to-background ratio (TBR) of 4:1 and diameter of 25 mm was placed in the base of right lung. The noise-free and noisy sinograms with attenuation modeling were generated and reconstructed with different noise-free and noisy AC maps (CACT, HCTs and IACTs) by STIR (Software for Tomographic Image Reconstruction) respectively, using OS-EM with up to 300 updates. Normalized-mean square error (NMSE), mutual information (MI), TBR and image profiles were analyzed. The PET reconstructed images with AC using CACT showed least difference as compared to the original phantom, followed by $IACT_{4o9i}$, $IACT_{2o11i}$, $IACT_{2s11i}$, HCT-5 and HCT-1/HCT-8. Significant artifacts were observed in the reconstructed images using HCTs for AC. The MI differences between $IACT_{2o11i}$ and $IACT_{4o9i}$/CACT were <0.41% and <2.17% respectively. With a slight misplacement of the two extreme phases, $IACT_{2s11i}$ was still comparable to $IACT_{2o11i}$ with difference of <2.23%. The IACT is a robust, accurate low dose alternate to CACT and works well for over 90% of the clinical patients.**

I. Introduction

Respiratory motion is generally considered the main problem in the CT-based attenuation correction (AC) in PET/CT. For conventional CT, a 3D helical acquisition of the thoracic cavity is collected over a single full-inspiration breath-hold CT scans. When applied with the emission exam, this technique captures a snapshot of the thoracic cavity in a distinct respiratory phase and does not represent the time-averaged position of the thoracic structures as PET acquisition does. In fact, for thoracic structures, more than 40% studies have misalignment between the measured and the true position [1]. Erdi *et al.* [2] have examined PET/CT images of 5 lung carcinoma patients with multiple lesions, and showed that spatial mismatch results in up to a 30% error in the standardized uptake value (SUV) of the lesions. Also, phantom studies showed the effect of motion can result in as much as 75% underestimation of the maximum activity concentrations [3]. These distortions may lead to inaccurate localization of tumors and hence potential misdiagnoses [4, 5].

Cine respiration-average CT (CACT) from a 4D CT acquisition for AC has been proposed to reduce the misalignment artifacts and improve quantification of PET/CT [6-8] as compared to the conventional helical CT (HCT). Previously we have developed an interpolated average CT (IACT) method, generated from the end-expiration and end-inspiration phases of cine CT and interpolated phases using deformable image registration, as a low dose alternate to CACT for AC in PET/CT [9]. We have demonstrated its clinical merits on 6 patients. This study aims to evaluate its accuracy and robustness, i.e. effects of different respiratory motion amplitudes and misplacement of the two extreme phases, based on computer simulations with known truth.

II. Materials and Methods

In this study, we simulated the sinograms with attenuation effects from the digital 4D Extended Cardiac Torso (XCAT) phantom (Fig. 1a) that realistically models the anatomy, activity distribution of a male patient injected with ^{18}F-FDG, and the respiratory motions. We used the analytical projector and OS-EM reconstruction algorithm provided by STIR (Software for Tomographic Image Reconstruction), modeling a GE Discovery STE PET scanner. The respiratory cycle was divided into 13 phases (Fig. 1b), starting from the end-inspiration phase, and three maximum respiratory diaphragm motions of 2 cm, 3 cm and 4 cm were modeled (Fig. 2). A spherical lesion with target-to-background ratio (TBR) of 4:1 and diameter of 25 mm was placed at the base of the right lung

Manuscript received November 15, 2011. This work was supported in part by the research grants of University of Macau (SRG004-FST11-MSP & MYRG185(Y1-L3)-FST11-MSP).

Greta S. P. Mok is with the Department of Electrical and Computer Engineering, Faculty of Science and Technology, University of Macau, Macau, People's Republic of China (telephone: (853) 8397-8465, e-mail: gretamok@umac.mo).

Tao Sun is with the Department of Electrical and Computer Engineering, Faculty of Science and Technology, University of Macau, Macau, People's Republic of China (e-mail: mb05470@umac.mo).

Tung-Hsin Wu is with the Department of Biomedical Imaging and Radiological Sciences, National Yang Ming University, Taiwan, Republic of China (e-mail: tung@ym.edu.tw).

Mu-Bai Chang is with the Graduate Institute of Clinical Medical Science, China Medical University, Taiwan, Republic of China (e-mail: white77830@hotmail.com).

Tzung-Chi Huang is with the Department of Biomedical Imaging and Radiological Sciences, China Medical University, Taiwan, Republic of China (e-mail: tzungchi.huang@mail.cmu.edu.tw).

which is close to the diaphragm, where the respiratory motion is more prominent.

The average of the 13 phases of the activity maps was used to generate the noise-free and noisy sinogram with added Poisson noise to represent PET acquisition with average of a respiratory cycle. For noise-free data, the CACT was represented by the average of the 13 phases of the attenuation maps. The HCT, which is usually a snapshot of a respiration cycle, was represented by phase #1 (end-inspiration phase), #5 (mid-respiratory phase) or #8 (end-expiration phase) of the attenuation maps (HCT-1, HCT-5 and HCT-8). The IACT was generated by averaging the original phases and the interpolated phases using deformable image registration. Three different IACTs were simulated: (1). 2 original extreme phases + 11 interpolated phases ($IACT_{2o11i}$), (2) 2 original phases right after the end-inspiration and -expiration phases + 11 interpolated phases ($IACT_{2s11i}$); and (3) 4 original phases (2 extreme and 2 mid-respiratory phases) + 9 interpolated phases ($IACT_{4o9i}$). For noisy CT data, CT projections were generated from different AC maps using an analytical projector and then added with Poisson noise based on the clinical patient data. The projections were reconstructed with filtered back-projection method to get the CT reconstruction images for further AC in PET.

The optical flow method (OFM), a deformable image registration algorithm, was applied to calculate the velocity matrix which includes lateral, anterior-posterior and inferior-superior displacement for each voxel on two successive CT phases in the respiratory cycle. The OFM calculation is as follows:

$$v^{(n+1)} = v^{(n)} + \nabla f \left(\frac{\nabla f \cdot v^{(n)} + \frac{\partial f}{\partial t}}{\alpha^2 + \|\nabla f\|^2} \right) \qquad (1)$$

where n is the number of iterations, $v^{(n)}$ is the average velocity driven from the surrounding voxels, f is the image intensity, and α is the weighting factor with empirical value of 5. The OFM was then used to generate the interpolated motion maps with the original phases for IACT.

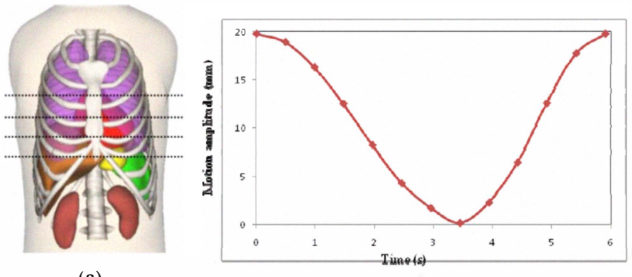

(a) (b)

Fig. 1. (a) The XCAT phantom and (b) the respiratory cycle was divided into 13 phases (2 cm maximum diaphragm motion was shown here).

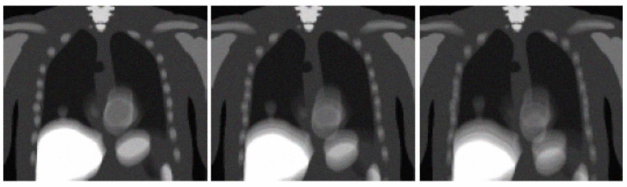

(a) (b) (c)

Fig. 2. The average activity maps showing (a) 2 cm and (b) 3 cm and (c) 4 cm maximum respiratory motions.

The noise-free and noisy PET sinograms were reconstructed using OS-EM algorithm with up to 300 updates. Attenuation corrections were conducted using noise-free and noisy HCTs, IACTs and CACT, respectively. Their reconstructed PET images were compared and analyzed in terms of the following indices:

(a) Normalized mean square error (NMSE)

The whole reconstructed volume was used to assess the average NMSE.

$$\text{average } NMSE = \frac{1}{n}\sum_{j=1}^{n}\left(\frac{x_j}{\bar{x}} - \frac{\lambda_j}{\bar{\lambda}}\right)^2 \qquad (2)$$

where n is the number of voxels in the whole reconstructed volume, λ is the voxel count value in the original phantom, $\bar{\lambda}$ is the mean voxel value of the original phantom, x is the voxel count value in the noise free and noisy reconstructed images, $\bar{x}$ is the mean voxel value of the reconstructed images and j is the voxel index.

(b) Mutual information (MI)

The normalized MI ($I(X, Y)$) between X and Y, a measure of the statistical dependence between both variables, was applied to estimate the nonlinear image intensity distribution between IACTs/HCTs/CACT and the original phantom:

$$I(X, Y) = P(X) + P(Y) / P(X, Y) \qquad (3)$$

where $P(X)$ is the histogram of X, $P(Y)$ is the histogram of Y and $P(X, Y)$ is the joint histogram of X and Y.

(c) Target-to-background ratio (TBR)

The 3D TBR was calculated from the known lesion region and the chosen background regions in the lung in reconstructed images using different CT maps:

$$TBR = \frac{\text{Mean}_{\text{hot lesion}}}{\text{Mean}_{\text{background}}} \qquad (4)$$

(d) Image profile

An image profile was drawn vertically across the lung, lesion and the diaphragm to demonstrate the misalignment artifacts in the reconstructed images (300 updates) using different CT maps.

III. RESULTS

From visual assessment, the IACTs modeled the respiratory motions similarly to the CACT (Fig. 3a).The PET reconstructed images with AC using CACT and IACT showed no significant artifacts as compared to the original phantom (Fig. 3b & 4). Significant artifacts were observed in the PET

reconstructed images using HCTs for AC (Fig. 3d & 4). For $IACT_{2o11i}$, the lesion movement cannot be modeled exactly for motion amplitude of 4 cm while it can be modeled for all motion amplitudes for $IACT_{4o9i}$ (Fig. 5). As in the visual assessment, the quantitative indices including NMSE, MI, TBR and image profiles showed that HCT-1 and HCT-8 had the worst performances for motion amplitudes of 2 cm and 3 cm (Fig. 6 & 7). As expected, reconstructed images using AC with CACT had least difference as compared to the original phantom for all quantitative indices, following by $IACT_{4o9i}$, $IACT_{2o11i}$, $IACT_{2s11i}$ and HCT-5 (Fig. 6 & 7). Our results showed that $IACT_{2o11i}$ provides similar accuracy as compared to $IACT_{4o9i}$ and even CACT, with MI difference of <0.41% and <2.17% respectively, reassuring our findings in the previous clinical studies. With a slight misplacement of these two phases, the resultant $IACT_{2s11i}$ still shows comparable accuracy to $IACT_{2o11i}$ with MI difference of <2.23%. Noise-free and noisy simulations have accordant results.

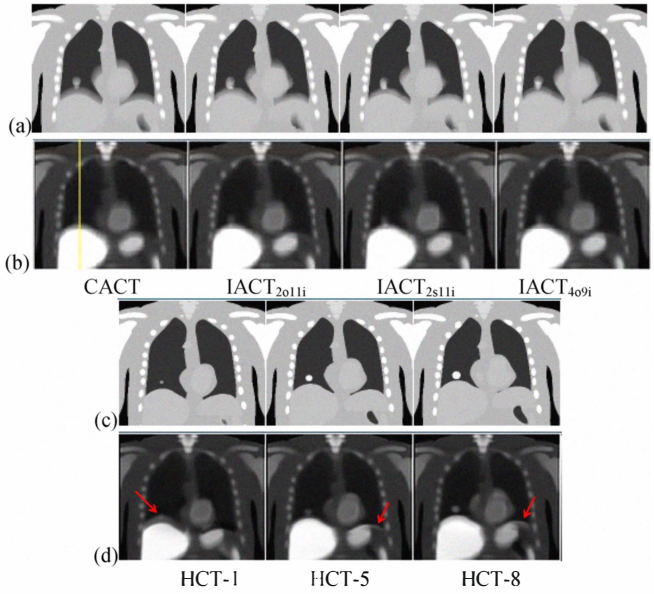

Fig. 3. (a) & (c) Different attenuation maps for AC and their corresponding PET reconstructed images (b) & (d) for respiratory motion= 2 cm. The yellow line indicates the position of the image profile. Significant misalignment artifacts were observed for the PET images using HCTs for AC (red arrows).

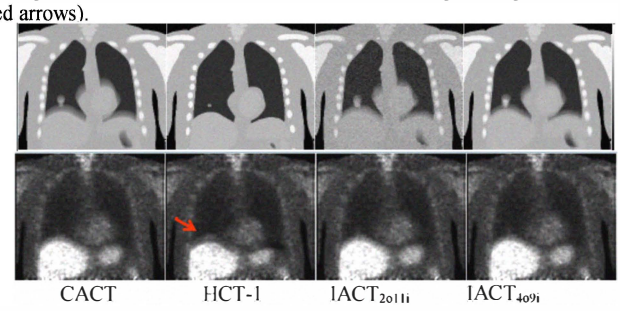

Fig. 4. Top row: different noisy attenuation maps for AC. Bottom row: their corresponding PET reconstructed images from noisy sinogram with 100 updates for maximum respiratory motion of 2 cm. Significant misalignment artifacts were observed for the PET images using HCTs for AC (red arrows)..

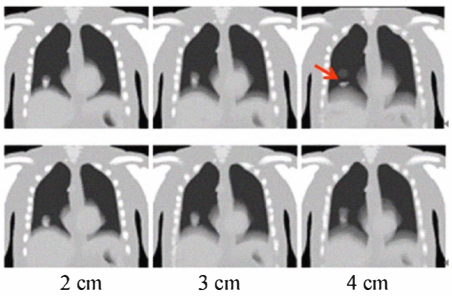

Fig. 5. Top row: $IACT_{2o11i}$ and bottom row: $IACT_{4o9i}$ maps for 3 different motion amplitudes. The lesion movement cannot be modeled correctly for $IACT_{2o11i}$ in motion= 4 cm (red arrow).

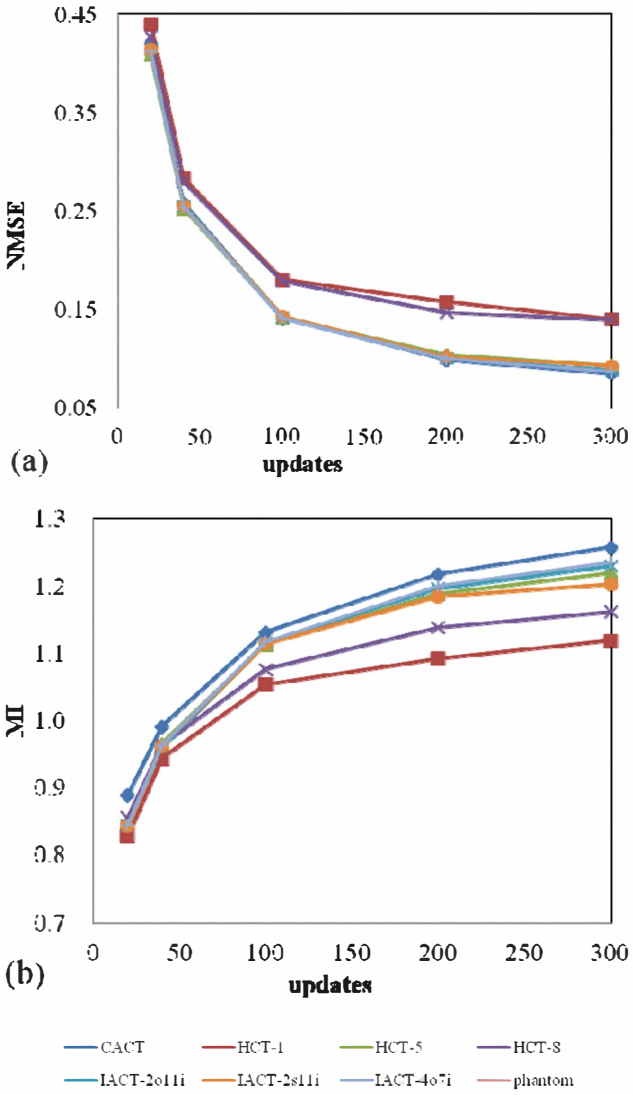

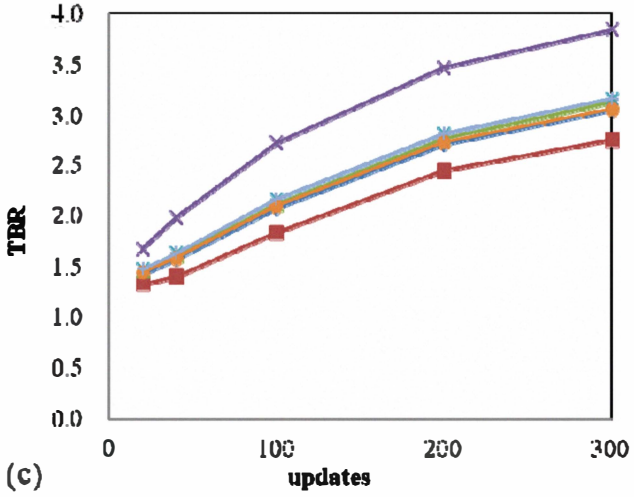
TBR
updates
(c)

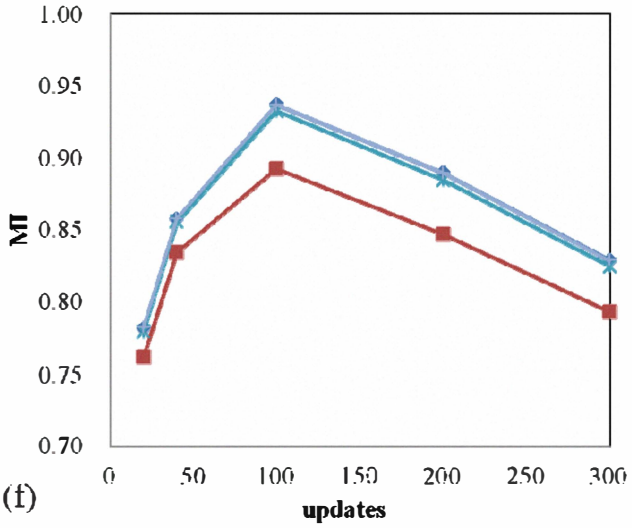
MI
updates
(f)

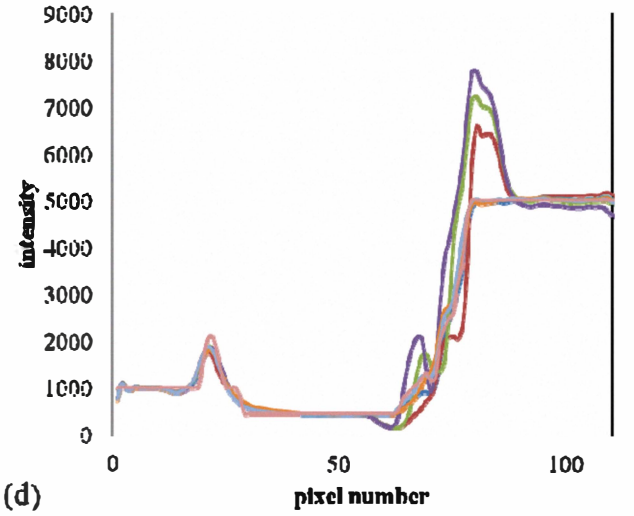
intensity
pixel number
(d)

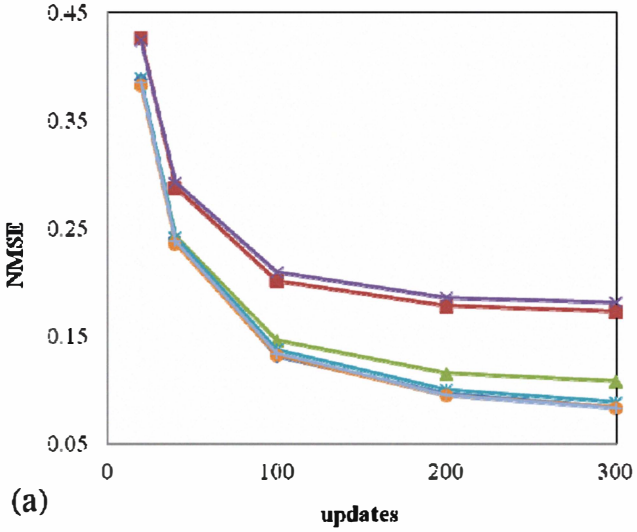
NMSE
updates
(a)

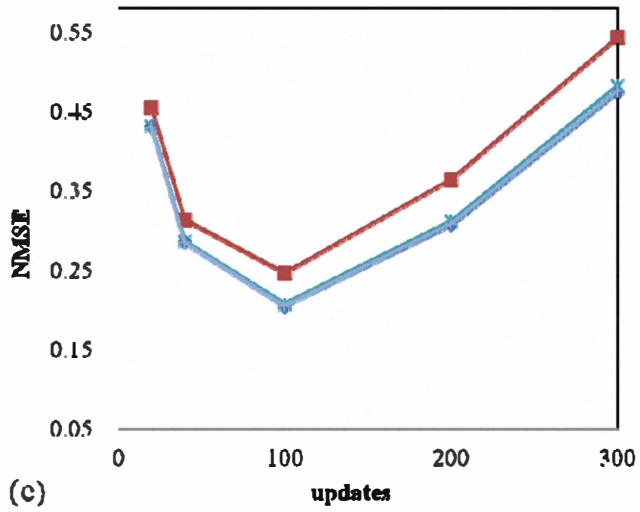
NMSE
updates
(c)

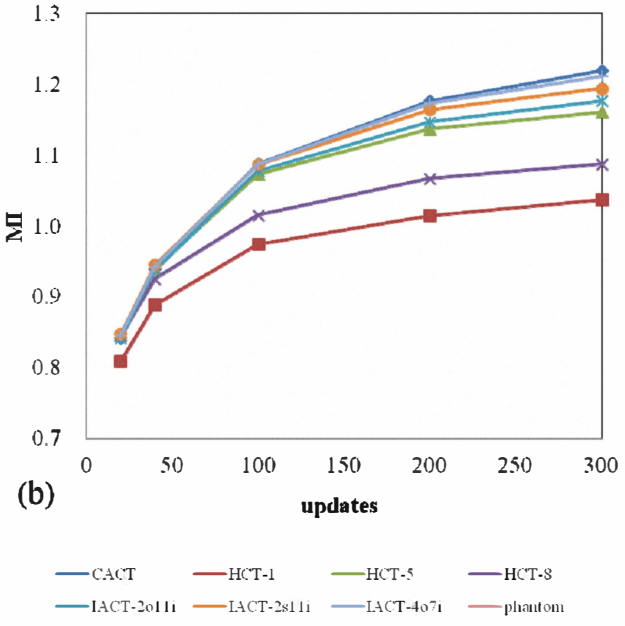
MI
updates
(b)
CACT
HCT-1
HCT-5
HCT-8
IACT-2o11i
IACT-2s11i
IACT-4o7i
phantom

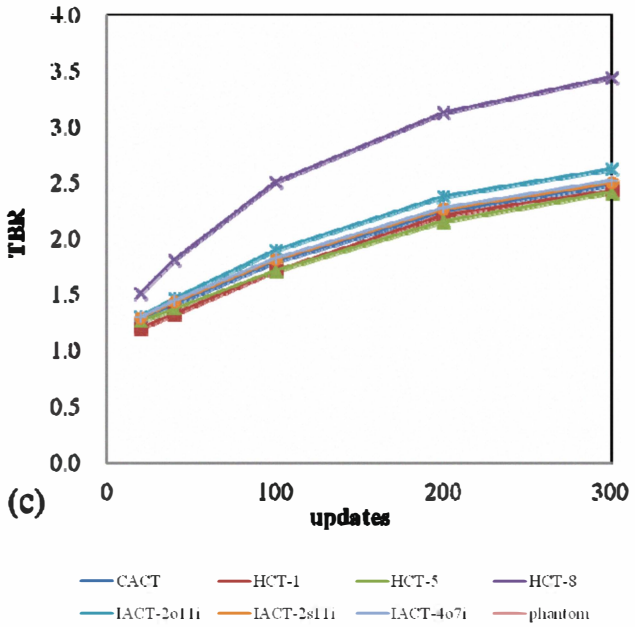

Fig. 7. Noise-free results of (a) NMSE, (b) MI and (c) TBR for respiratory motion of 3 cm.

IV. DISCUSSION

One limitation for our study is that the HCT we simulated represented a free-breathing state, i.e. the CT acquired when the patients did not take any breath-hold. Thus, one can infer that the improvement of IACT as compared to realistic breath-hold HCT would be more significant. Among HCTs, HCT-5 showed the best performance in this study, which matched with our predictions that mid-phase HCT is probably more similar to CACT as compared to conventional breath-hold CTs (HCT-1 and HCT-8). However, quantitative indices generally showed that HCT-5 worked slightly inferior to the IACTs. Also, it is clinically difficult to assure that the HCT-5 (mid-phase of the respiratory cycle) would be captured for the HCT acquisition. Different breathing patterns for CT acquisition in PET/CT are now being explored, including normal-expiration breath-hold [10, 11] and deep-inspiration breath hold [12].

Our results showed that IACT method using 4 original phases ($IACT_{4o9i}$) works well for maximum breathing motion amplitude of 4 cm, covering ~95% of patients [7]. Though the IACT method using 2 original phases ($IACT_{2o11i}$) works well for motion amplitude of ~3 cm, it stills cover ~90% of the clinical patients [7]. Our previous work suggested generating the IACT using just the free breathing end-expiration and end–inspiration phases, i.e. 2 phases, to minimize the dose. It may also be feasible to achieve the same dose reduction with improved image quality using more phases for interpolation by reducing the dose for each phase, as our current study hints that $IACT_{4o9i}$ works well for larger motion amplitude and more closely mimics CACT.

V. CONCLUSIONS

In this study, we have evaluated and analyzed the effectiveness of IACT as compared to CACT and HCT using simulations. We concluded that IACT is a robust, accurate low dose alternate to CACT and works well for a large range of respiratory motion amplitudes. Further optimization of IACT protocol with the consideration of dose reduction is warranted.

ACKNOWLEDGMENT

The authors thank Dr. Jinyan Xu from Division of Medical Imaging Physics at Johns Hopkins University for her suggestions on CT noise modeling.

REFERENCES

[1] K. L. Gould, T. Pan, C. Loghin, N. P. Johnson, A. Guha, and S. Sdringola, "Frequent diagnostic errors in cardiac PET/CT due to misregistration of CT attenuation and emission PET images: a definitive analysis of causes, consequences, and corrections," *J Nucl Med,* vol. 48, pp. 1112-21, Jul 2007.

[2] Y. E. Erdi, S. A. Nehmeh, T. Pan, A. Pevsner, K. E. Rosenzweig, G. Mageras, E. D. Yorke, H. Schoder, W. Hsiao, O. D. Squire, P. Vernon, J. B. Ashman, H. Mostafavi, S. M. Larson, and J. L. Humm, "The CT Motion Quantitation of Lung Lesions and Its Impact on PET-Measured SUVs," *Journal of Nuclear Medicine,* vol. 45, pp. 1287-1292, August 1 2004.

[3] A. Pevsner, S. A. Nehmeh, J. L. Humm, G. S. Mageras, and Y. E. Erdi, "Effect of motion on tracer activity determination in CT attenuation corrected PET images: A lung phantom study," *Medical Physics,* vol. 32, p. 2358, 2005.

[4] G. Cook, E. Wegner, and I. Fogelman, "Pitfalls and artifacts in FDG PET and PET/CT oncologic imaging," *Seminars in Nuclear Medicine,* vol. 34, pp. 122-133, 2004.

[5] M. M. Osman, C. Cohade, Y. Nakamoto, L. T. Marshall, J. P. Leal, and R. L. Wahl, "Clinically Significant Inaccurate Localization of Lesions with PET/CT: Frequency in 300 Patients," *Journal of Nuclear Medicine,* vol. 44, pp. 240-243, February 1 2003.

[6] T. S. Pan, O. Mawlawi, D. Luo, H. H. Liu, P. C. M. Chi, M. V. Mar, G. Gladish, M. Truong, J. Erasmus, Z. X. Liao, and H. A. Macapinlac, "Attenuation correction of PET cardiac data with low-dose average CT in PET/CT," *Medical Physics,* vol. 33, pp. 3931-3938, Oct 2006.

[7] T. S. Pan, C. Mawlawi, S. A. Nehmeh, Y. E. Erdi, D. S. Luo, H. H. Liu, R. Castillo, R. Mohan, Z. X. Liao, and H. A. Macapinlac, "Attenuation correction of PET images with respiration-averaged CT images in PET/CT," *Journal of Nuclear Medicine,* vol. 46, pp. 1481-1487, Sep 2005.

[8] R. A. H. Cook, G. Carnes, T. Y. Lee, and R. G. Wells, "Respiration-averaged CT for attenuation correction in canine cardiac PET/CT," *Journal of Nuclear Medicine,* vol. 48, pp. 811-818, May 2007.

[9] T. C. Huang, G. S. P. Mok, S. J. Wang, T. H. Wu, and G. Zhang, "Attenuation correction of PET images with interpolated average CT for thoracic tumors," *Physics in Medicine and Biology,* vol. 56, pp. 2559-2567, Apr 21 2011.

[10] E. K. T.-N. H. G. W. Goerres, "PET-CT image co-registration in the thorax: influence of respiration," *Eur J Nucl Med Mol Imaging,* vol. 29, pp. 351-360, 2002.

[11] G. W. Goerres, E. Kamel, B. Seifert, C. Burger, A. Buck, T. F. Hany, and G. K. von Schulthess, "Accuracy of Image Coregistration of Pulmonary Lesions in Patients with Non-Small Cell Lung Cancer Using an Integrated PET/CT System," *Journal of Nuclear Medicine,* vol. 43, pp. 1469-1475, November 1 2002.

[12] G. S. Meirelles, Y. E. Erdi, S. A. Nehmeh, O. D. Squire, S. M. Larson, J. L. Humm, and H. Schoder, "Deep-inspiration breath-hold PET/CT: clinical findings with a new technique for detection and characterization of thoracic lesions," *J Nucl Med,* vol. 48, pp. 712-9, May 2007.